Quantitative and geomorphologic parameterization of megaclasts within mass-transport complexes, offshore Taranaki Basin, New Zealand

Wei Li[a, b, c]*, Yan Li[a, c]*, Kamaldeen O.L Omosanya[d, e, f], Tiago M. Alves[g], Song Jing[a], Nan Wu[h], Xiujuan Wang[i], Wenhuan Zhan[a, b, c]

[a] CAS Key Laboratory of Ocean and Marginal Sea Geology, South China Sea Institute of Oceanology, Chinese Academy of Sciences, Guangzhou 510301, China

[b] Southern Marine Science and Engineering Guangdong Laboratory (Guangzhou), 511458, P.R. China

[c] University of Chinese Academy of Sciences, Beijing 100049, P.R. China

[d] Oasisgeokonsult, 7052 Trondheim, Norway

[e] Norwegian University of Science and Technology, Norway.

[f] Department of Geoscience, University of Malta. Msida.

[g] 3D Seismic Lab. School of Earth and Ocean Sciences, Cardiff University, Main Building, Park Place, Cardiff, CF10 3AT, United Kingdom

[h] Tongji University, State Key Laboratory of Marine Geology, Shanghai 200092, China

[i] Laboratory for Marine Mineral Resources, Qingdao National Laboratory for Marine Science and Technology, Qingdao, 266071, China

*Corresponding author: Yan Li (liyan191@mails.ucas.ac.cn) and Wei Li (wli@scsio.ac.cn)

Highlights

- Large-scale megaclasts are identified and analyzed in seismic data .

- A new classification of megaclasts is proposed based on their deformational styles.

- The identified megaclasts reflect two types of emplacement processes.

- Internal structures in megaclasts reflect their emplacement histories.

Abstract

Mass-transport complexes (MTCs) in sedimentary basins reflect the gravitational transport of sediments from the shelf edge to the abyssal plain. As an integral part of MTCs, megaclasts (large sedimentary blocks of 100s of meters long) can record kinematic and sedimentary information deemed essential to understand source-to-sink systems. Yet, deformation structures in such megaclasts remain poorly understood. This study uses high-quality three-dimensional (3D) seismic reflection data from the deep-water Taranaki Basin offshore New Zealand to analyze the morphological character of 123 megaclasts and propose a new classification scheme based on their morphometric properties. The megaclasts are up to 400 m tall, 1900 m long and 1200 m wide. In the study area, they are high- to moderate-amplitude features owing to their different lithology and continuous to contorted seismic facies. The megaclasts can be classified as undeformed, rotated, deformed, and highly deformed based on their internal deformational styles. Two different kinds of morphological depressions observed on their basal shear zones further indicate that the megaclasts are either transported or formed in-situ. Our study demonstrates that the quantitative parameterization of the megaclasts provides important information on their deformational processes, helping a more complete understanding of megaclast emplacement along continental margins.

Keywords: Mass-transport complexes, megaclasts, deformational styles, quantitative analysis, classification, deep-water Taranaki Basin.

1. Introduction

Submarine mass-wasting is widely observed on continental margins as a primary process transporting large volumes of sediment from continental shelves to deep-water sedimentary basins (Hampton et al., 1996; Nisbet and Piper, 1998; Canals et al., 2004; Moscardelli and Wood, 2008). Megaclasts are large blocks preserved within the sedimentary deposits resulting from submarine mass wasting (Moore et al., 1995; Lee et al., 2006; Vanneste et al., 2006; Alves, 2015; Gamboa and Alves, 2015; Ogata et al., 2019). Megaclasts can be 100s of meters to kilometers long and/or wide (Alves, 2015; Hodgson et al., 2019; Nwoko et al., 2020b; Hunt et al., 2021) and have been documented in multiple deep-water regions such as offshore Brazil (Alves and Cartwright, 2009; Jackson, 2011; Omosanya and Alves, 2013; Gamboa and Alves, 2015), offshore New Zealand (Collot et al., 2001; Joanne et al., 2013; Rusconi, 2017; Kumar et al., 2021), around the island of Anak Krakatau (Hunt et al., 2021), in the Southwest Labrador Sea (Deptuck et al., 2007), in the Arctic Ocean (Vanneste et al., 2006) and in the Central North Sea (Soutter et al., 2018) (Fig. 1).

Megaclasts can create uneven topographies at the top surface of mass-transport complexes (MTCs), influencing the subsequent flows (e.g., turbidity currents) and their deposits (Ward et al., 2018; Nwoko et al., 2020a). Relative to their surrounding host strata, megaclasts have much stiffer geotechnical properties (higher density and lower porosity), promoting differential compaction under variable overburden pressures (Soutter et al., 2018; Ward et al., 2018; Cox et al., 2020). This differential compaction can lead to the formation of structural traps in younger strata above the megaclasts and often influence the seafloor physiography 1000s of years later (Alves and Cartwright, 2009; Alves, 2010). Megaclasts also have a recognized erosional potential as they are capable of generating grooves and striations on their basal shear zones Gee et al., 2005; Soutter et al., 2018; Scarselli, 2020; Kumar et al., 2021). Importantly, the internal structures of megaclasts usually record a continuum of deformational styles, which are important to estimate the flow directions of MTCs (Jackson, 2011; Gamboa and Alves, 2015; Rusconi, 2017; Omeru and Cartwright, 2019; Nwoko et al., 2020b).

The deep-water Taranaki Basin provides a natural laboratory to investigate the internal architecture of megaclasts. Five MTCs (MTC 1 to 5 from bottom to top) have been recognized in the deep-water Taranaki Basin offshore New Zealand (Kumar et al., 2021). One of them (MTC 2) contains multiple megaclasts that are up to 1900 m long (Omeru and Cartwright, 2019; Bull et al., 2020; Kumar et al., 2021). Previous studies in the Taranaki Basin have mainly focused on the distribution, internal architecture and kinematic indicators of these MTCs and their roles on post-MTC sedimentation (Omeru and Cartwright, 2019; Bull et al., 2019, 2020; Nwoko et al., 2020a). However, few researchers have concentrated on the megaclasts within MTCs (e.g., Nwoko et al., 2020b; Kumar et al., 2021). Despite the relevant information provided by megaclasts, little knowledge exists on their dynamics vis-à-vis emplacement processes. Only a few studies have concentrated on the internal structures of megaclasts, and these are purely limited to simple correlations between the styles of deformation in megaclasts and their sliding directions and distances (e.g., Jackson, 2011; Alves, 2015; Cardona et al., 2020; Ogata et al. 2020).

In this study, we use 3D seismic data to investigate the deformational styles, origin and emplacement processes of megaclasts within MTC 2 (Figs. 2，3 and 4). To achieve these aims we: a) analyze their geometry, scale, distribution and internal seismic character; b) quantitatively classify the megaclasts based on their different deformational styles, and c) propose a schematic model to explain their emplacement process.

2. Geological setting of the Taranaki Basin

The Taranaki Basin is one of the largest Cretaceous-Cenozoic sedimentary basins offshore New Zealand, covering an area of ~330 km^2 (Fig. 2). It is located ~190 km west of the North Island to the west of the Australia-Pacific plate boundary zone (Fig. 2; Strogen et al., 2017). The study area is located in the northeastern part of the Taranaki Basin, at water depths of 1000-1800 m, in the so-called deep-water Taranaki Basin (Fig. 2). The basin is itself is related to the subduction of the oceanic Pacific Plate under the continental Australian Plate (Fig. 2; Beavan et al., 2002; Giba et al., 2010; Infante-Paez and Marfurt, 2017). As a back-arc rift depocenter, the Taranaki Basin has experienced a complex tectonic evolution (King and Thrasher, 1992; Giba et al., 2010) that includes three major stages of deformation: an extensional stage from the Cretaceous to the Paleocene (~84-55 Ma), a shortening stage from the Eocene to Recent (~40-0 Ma), and a period of intense volcanism from the Late Miocene to Recent (~12-0 Ma) (Giba et al., 2010; Infante-Paez and Marfurt, 2017). Two extensional episodes occurred in the Taranaki Basin from the Cretaceous to the Paleocene: the Zealandia rifting and the West Coast-Taranaki rifting (Infante-Paez and Marfurt, 2017). They caused localized fault-controlled extensional subsidence, contributing to the development of graben and half-graben sub-basins (King and Thrasher, 1992; Stagpoole and Nicol, 2008).

As for the depositional history of the Taranaki Basin, rapid sedimentation occurred from Late Cretaceous to Early Miocene, with up to 8 km of sediments having been deposited during a transgressive-regressive cycle (King and Thrasher, 1992). The transgressive phase reached its climax in the Early Miocene with the deposition of calcareous mudstones in the Taimana Formation, and siltstones in the Manganui Formation (King and Thrasher, 1992; Cooper et al., 2001). The regressive phase started in the Mid-Miocene and continues to the present day (Higgs et al., 2012). Tectonic compression affecting the northern part of the Taranaki Basin ceased in the Middle Miocene, resulting in the formation of a submarine volcanic arc – the Mohakatino arc – and concomitant deposition of sandstones (Moki Formation) and siltstones in the Manganui Formation (Fig. 3; Holt and Stern, 1994; Hansen and Kamp, 2002; Kamp et al., 2004). A thick, mud-dominated progradational succession, the Giant Foresets Formation, was deposited during the Plio-Pleistocene in the shallower parts of the basin (Fig. 3; Hansen and Kamp, 2006).

Mass wasting is prevalent within the Taranaki Basin, and five large-scale MTCs (MTC 1 to 5) have been documented in the late Miocene to Pleistocene succession based on the Romney-1 well (Fig. 3; Rad, 2015). These MTCs can represent more than 50% of the near-surface stratigraphic column. Based on the correlation between interpreted horizons and the regional geological lithostratigraphy, megaclasts in MTC 2 are likely Late Miocene in age (Bull et al., 2020; Kumar et al., 2021). They were sourced from the shallower outer shelf and upper slope of the North Island of New Zealand and reveal a north-westerly transport direction (Bull et a., 2019). The triggers for the MTCs are still unclear, but MTC 1-4 were likely affected by the high sedimentation rates recorded in the basin, while the collapse of MTC 5 is related to overpressure build-up (Omeru, 2014).

3. Data and methods

3.1 Romney 3D survey and Romney-1 well

The primary dataset used for this study is the Romney 3D survey acquired by the Ministry of Business, Innovation and Employment of New Zealand in 2011. This survey covers an area of approximately 1925 km^2 in the northeastern part of the Taranaki Basin, offshore New Zealand (Fig. 2). The 3D seismic data has a sampling interval of 4 ms and its bin size is 12.5 m × 25 m. As the interval of interest has a velocity of 1850 m/s and a dominant frequency of 41 Hz (Rusconi, 2017), the vertical resolution of strata in the studied MTCs is ~ 11.25 m. Exploration well Romney-1 is located in the north of the study area and drilled through a 4594 m-thick clastic succession (Rusconi, 2017). In this work, interpreted seismic horizons were tied to the seismic data using well Romney-1 and information taken from the well-defined regional lithostratigraphic frameworks of Rusconi (2017) and Nwoko et al. (2020a) (Fig. 3).

3.2 Seismic interpretation

The approach followed in this work includes a detailed seismic-stratigraphic interpretation complemented by the compilation of time-structure and seismic-attribute maps (sensu Mitchum et al., 1977). Based on seismic-well ties and published information (e.g., Bull et al., 2020), eight laterally continuous seismic horizons are mapped in this work (Fig. 3b). Seismic interpretation is based on the standard industry software Petrel® from Schlumberger.

We focus on the Upper Miocene to Holocene formations of the Taranaki Basin, in which five MTCs (MTCs 1-5) are imaged (Figs. 3 and 4). The Upper Miocene to Holocene strata are delimited by Horizon N60-4 and the seafloor (Fig. 3) and reflect the relatively fast deposition of fine-grained sandstones (~30 cm/kyr; King and Thrasher, 1992; Scott et al., 2004; Strogen et al., 2019). Isochron maps at the top MTC 2 were generated to highlight the location of megaclasts and assess their influence on subsequent flows. The basal shear zone of MTC 2 was also mapped to reveal any interactions amongst the megaclasts and their underlying strata.

3.3 Calculations of deformation within megaclasts

The deformation of discrete megaclasts refers to: (a) internal deformation and (b) angle of external rotation, two parameters quantified based on morphological analysis of the megaclasts' internal reflections (Fig. 5). Along their sliding direction, the length of curved line (LCL) and the length of straight line (LSL) were measured in megaclasts to obtain their aspect ratio (LCL/LSL) (Fig. 5b). Here, the degree of internal deformation within megaclasts (DID) corresponds to LCL/LSL minus 1 (LCL/LSL-1), i.e., a measure of whether the megaclasts comprise parallel, convex-up or concave-up strata (Fig. 6). If the internal reflections within megaclasts are convex-up, the ratio of DID is positive (DID >0). Conversely, DID is negative (DID <0) when the internal reflections in the megaclasts are concave-up. If the internal reflections in the megaclasts are parallel, then DID is 0.

The angle of external rotation (θ) reflects the degree of rotation of the megaclasts and is derived using the relationship between the straight line of the two endpoints of the same reflection axis and the horizontal (Fig. 5b). Here, we define that point "B" is higher than point "A" and use point B as the intersection point when calculating the external rotation of megaclasts. The angle is positive ($\theta>0$)

when the inclination of the reflection axis is consistent with the sliding direction (e.g., Fig. 5b), otherwise $\theta<0$.

4. Megaclasts within mass-transport complexes

Five MTCs are interpreted in the study area and comprise low-amplitude, semi-transparent to chaotic seismic reflections grouped into blocky and non-blocky MTCs (Fig. 4; Table 1). Blocky MTCs show parallel to slightly deformed, high-moderate amplitude seismic reflections embedded within a seismically chaotic matrix of the MTCs (Figs. 4 and 6).

On the structural map of MTC 2, blocks have principal axes that are 10s of meters to several kms long (Figs. 4 and 6). They are interpreted as megaclasts based on their scales (e.g., Jackson, 2011; Omosanya and Alves, 2013; Alves, 2015; Nwoko et al., 2020b). Many locally moderate- to low-amplitude megaclasts are also identified in other MTCs (Fig. 4). However, megaclasts in MTC 2 display higher diversity of internal deformation when compared to other MTCs in the study area. Well Romney-1 shows that MTC 2 occurs in Miocene strata and comprises rotated slumps in claystone and mudstone intervals. At the top of the MTC lies a ~25 m-thick sandstone interval, while its base contains several sandstone intervals grading into calcareous rocks (Fig. 3b).

4.1 Geometry, scale and distribution of megaclasts in MTC 2

In total, 123 megaclasts with clear boundaries and visible internal reflections are identified in MTC 2 (Fig. 7a). Here, they are described based on their scale, internal stratigraphy and morphological characters. The longest axis (L) of megaclasts is 400 m to 2000 m, whereas their shortest axis (W) varies from 300 m to 1200 m (Figs. 5a and 7b). The average length and width of megaclasts are ~1000 m and ~620 m, respectively (Figs. 5a and 7b). Their height (H) ranges from 150 to 400 m with an average value of ~250 m (Figs. 5a and 7b). Overall, the height of the megaclasts increases from southeast to northeast (Fig. 4).

4.2 Top surface and basal shear zone of MTC 2

The top surface of MTC 2 is a high-amplitude positive reflection with a similar polarity to the seafloor reflection (Figs. 4 and 6). Some of the largest megaclasts, greater than the thickness of MTC 2 at the considered point of observation, pierce the top of the MTC in the NE and SW to generate an irregular top surface with local relief (Figs. 4, 6, 8 and 9a-b). The basal shear zone of MTC 2 is a low-amplitude seismic reflection with a negative polarity (Figs. 4 and 6). Compared with the top surface, the basal shear zone of MTC 2 is relatively flat, with gradients as low as ~1° (Figs. 4 and 8b). Several linear grooves can be observed at the basal shear zone of MTC 2 and show an orientation of NWW-SEE with a width of 300~330 m and a length of up to 18 km (Fig. 8b).

The basal shear zone of MTC 2 shows two types of depressions below the megaclasts (Figs. 8b and 9c-d). Type I depressions are mostly found in the NE and SW of the study area (Fig. 8b). Type I depressions are U-shaped in map view and open toward the SE, a character consistent with the sliding direction of MTC 2 (Figs. 9c and 10a). Type I depressions have widths and lengths similar to the overlying megaclasts. For example, one Type I depression in the northeast is ~1211 m wide, ~1500 m long, and up to 50 m deep (Figs. 9c, e and f). The megaclast overlying this Type I depression has a length of 1000 m and a maximum height of 250 m, and its edge aligns with the boundary of the underlying depression (Figs. 9a and c). This megaclast is deformed with overall concave-up and forward-dipping internal reflections, with a DID of 0.05 and an external rotation of 15.17° (Fig. 10c).

Type II depressions are mainly found in the northwest part of MTC 2 (Figs. 8b and 9d). Type II depressions are circular-, oval- or irregular-shaped (Figs. 9d, g, h and 10b). The shapes of Type II depressions are entirely consistent with the boundaries of overlying megaclasts (Fig. 8). For instance, one Type II depression found in the northwest part of the study area is 1244 m wide, 1311 m long and ~45 m deep (Figs. 9d, e, f, and 10b). The overlying megaclast has exactly the same morphometric values, despite being slightly deformed, with a DID of -0.009 and internal strata typically forward-dipping at 11.99° (Fig. 10d).

4.3 Classification of megaclasts based on morphometric parameters

Based on their angle of rotation and degree of internal deformation, the megaclasts in the study area are further divided into undeformed, rotated, deformed, and highly deformed types (Figs. 11 and 12). Their character is described as follows:

(1) Undeformed megaclasts (DID = 0, $\theta = 0$) comprise undeformed and non-rotated reflections and quantitatively correspond to the planar-aclinic type (Fig. 11c). Undeformed megaclasts can also be termed as remnant or in-situ megaclasts with no evidence for movement (i.e., Alves, 2015). Thus, no basal and internal deformation features are observed.

(2) Rotated megaclasts (DID = 0, $\theta > 0$ or $\theta < 0$) show rotated internal reflections (Figs. 11a and b). Based on the angle of rotation (θ) alone, the rotated megaclasts are further subdivided into planar-forward dipping megaclasts (PF megaclasts, $\theta > 0$; Fig. 11a) and planar-backward dipping megaclasts

(PB megaclasts, θ < 0; Fig. 12b). The PF megaclasts (DID = 0, θ > 0) show rotated internal reflections, and the direction of rotation is the same as their sliding direction (Fig. 11a). PB megaclasts (θ < 0, DID = 0) show rotated internal reflections whose direction of rotation is opposite to their sliding direction (Fig. 11b).

(3) Deformed megaclasts (θ = 0, DID ≠ 0) are syncline-aclinic (SA) megaclasts and anticline-aclinic (AA) megaclasts (Figs. 11f and i). SA megaclasts (Fig. 11f) show small-scale concave-up reflections (θ = 0 and DID > 0), while AA megaclasts (Fig. 11i) have convex-up reflections (θ = 0 and DID < 0), reflecting syncline and anticline deformations, respectively.

(4) Highly deformed megaclasts (DID > 0 or DID < 0, θ >0 or θ < 0) have deformed and rotated reflections including syncline-forward (SF) dipping, syncline-backward (SB) dipping, anticline-forward (AF) dipping, and anticline-backward (AB) dipping megaclasts (Figs. 11d, e, g and h). SF megaclasts (DID > 0 and θ > 0) show bent-down internal reflections and are rotated towards their sliding direction (Fig. 11d). Internal reflections of SB megaclasts (DID > 0 and θ < 0) are rotated opposite to their sliding direction (Fig. 11e). AF megaclasts (DID <0 and θ > 0), showing anticline and backward dipping reflections (Fig.11g), are rotated in their sliding direction (Figs. 11g and h). Highly deformed megaclasts are most common in MTC 2 and can reach up to 80% of the total amount of mapped megaclasts (Fig. 12).

5 Discussion

Our observations and interpretations on the deformational styles and basal shear zones of the megaclasts within MTC 2 enable us to better understand their origin and emplacement processes.

This section starts with a discussion on the source of these megaclasts. Secondly, a discussion follows on how the different emplacement processes affect the deformational styles of megaclasts.

5.1 Source of megaclasts: transported or in-situ?

Megaclasts in mass-transport complexes have been widely studied and proposed to be derived from: a) fragmented strata derived from the headwall region of landslides (Moore et al., 1995; Huvenne et al., 2002; Alves and Cartwright, 2009; Ortiz-Karpf et al., 2017; Wu et al., 2021); b) collapsed strata along the lateral margins of MTCs (Alves, 2010; Joanne et al., 2013; Hodgson et al., 2019); or (c) basal shear zones (Ortiz-Karpf et al., 2015; Hodgson et al., 2019). Regardless of their provenance or size, blocks within MTCs can generally include transported and remnant types (Gamboa et al., 2012; Alves, 2015; Omosanya, 2018).

Two types of megaclasts can be determined based on the different depressions they left on the basal shear zone (Figs. 8b, 10a and b, Table. 2). It is worth noting that Type I megaclasts are characterized by the presence of U-shaped depressions at their basal shear zones and these depressions are aligned with the sliding direction and the boundaries of their overlying megaclasts (Figs. 8b, 9c, 9e and 9f). These U-shaped depressions are much wider than the classical grooves and/or striations observed at the base of MTCs, which are key kinematic indicators on the orientation of MTCs (e.g., Gee et al., 2005). Seismic profiles crossing Type I megaclasts show obvious truncations along their basal shear zone (Fig. 10c). This suggests that these megaclasts have severely eroded the underlying strata (e.g., Gee et al., 2005; Draganits et al., 2008; Joanne et al., 2013; Nwoko et al., 2020b), leading to the formation of U-shaped depressions. Therefore, Type I megaclasts with U-shaped depressions at their basal shear zones are considered to be transported megaclasts.

Compared to the Type I megaclasts with U-shaped depressions, several Type II megaclasts in the west of our study area are characterized by circular-, oval- or irregular-shaped depressions (Fig. 8b). These depressions have similar dimensions to the boundaries of overlying megaclasts (Fig. 8b, 9d, g and h). The seismic reflections below the base of the megaclasts are continuous (Fig. 10d), suggesting the absence of erosion along their basal shear zone. As for the origin of this kind of megaclasts, one interpretation is that they were buoyant due to the presence of sufficient debris-flow matrix and they would not leave grooves and striations on the basal shear zone of MTCs (e.g., Gee et al., 2005; Joanne et al., 2013). According to Johnson (1970), whether the megaclasts can be buoyant or not depends on the yield strength (a critical rheological parameter) of the debris flow, which affects the flow transporting competence. The dimension of Type II megaclasts is larger than the nearby Type I megaclasts (Figs. 4 and 8b, Table 2). If the Type II megaclasts can be buoyant, then the adjacent ones with smaller sizes should also have been buoyant and transported by the debris flows. However, the smaller-scale Type I megaclasts have obvious U-shaped depressions at their bases, suggesting that the larger Type II megaclasts were not buoyant within moving debris flows.

The second hypothesis for the source of Type II megaclasts is that they might be derived from in-situ strata (e.g., Ortiz-Karpf et al., 2015). Compared to the transported megaclasts, strata at the bottom of the Type II megaclasts are continuous and their internal reflections are slightly deformed (Fig. 10d). This observation also suggests that these megaclasts would have not undergone obvious transportation (e.g., Masson et al., 1993; Hodgson et al., 2019). Following this hypothesis, the megaclasts with Type II depressions are, therefore, considered as remnant megaclasts, or reflecting limited transport distance.

5.2 Deformational styles and emplacement processes of megaclasts

Megaclasts within MTC-related debris flows can be deformed, and this is related to local differential shear within the debris flows and subsequent interaction with the basal shear zone (Bull et al., 2009; Alves, 2015). The investigated megaclasts in MTC 2 show various deformational styles, including undeformed, rotated, deformed and highly deformed megaclasts (Fig. 12). These different deformational styles may provide kinematic indicators related to the initiation, motion and arrest of the debris flows (e.g., Lucente and Pini, 2003; Bull et al., 2009) and can also be used to infer the emplacement processes of megaclasts (Fig. 13; e.g., Jackson, 2011).

Two different types of megaclasts have been determined in the previous section, i.e., transported (Type I) and remnant (Type II) megaclasts. In general, the dimension (height, length and width) of transported megaclasts is observed to decrease along the sliding direction (Fig. 4), and their average height is 7.6% smaller than the remnant megaclasts (Table 2). During sliding, megaclasts are likely affected by friction and their bottom surfaces can be abraded along the basal shear zone (Fig. 13b; Moore et al., 1995; Tinti et al., 1997; Alves and Cartwright, 2009; Alves, 2010; Ogata et al., 2014; Soutter et al., 2018; Hodgson et al., 2019). This would make the heights of transported megaclasts decrease, leading to the formation of faults within them (Fig. 4). As the sliding distance increases, faults within the megaclasts may gradually develop until they penetrate and deform the entire megaclasts, resulting in their disintegration into smaller pieces with a decrease in their dimensions downslope (Fig. 4; e.g., Alves and Cartwright, 2009; Ogata et al., 2014; Ortiz-Karpf et al., 2017; Hodgson et al., 2019).

Our observations show that almost all the transported megaclasts have been tilted, regardless of their forward- or backward-dipping geometry (Table 3). One explanation for this marked tilting of megaclasts is that they might be influenced by the surrounding debris flows. Megaclasts are transported downslope together with debris flows and they can be partially pushed and dragged by the latter (e.g., Lastras et a., 2005). This would lead to the formation of forward-dipping megaclasts and abrasion would occur in their frontal parts. Our results also show that the forward-dipping transported megaclasts are larger than the backward-dipping ones (Table 4). If the larger megaclasts can be forward-dipping under the influence of debris flows, then the smaller megaclasts should have also been tilted forward. However, this interpretation contradicts our previous observations (Table 4). Thus, we do not think that the debris flows have played a vital role in the tilting of megaclasts. The most likely reason to explain the tilting of megaclasts is that the paleo-seafloor is not smooth and megaclasts interacted with the rugged paleo-seafloor when moving downslope. This interaction was capable of enhance erosion in the front or back of the megaclasts, generating forward- or backward-dipping strata in their interior (Figs. 7a, 13a-b and Table 5). In addition, most of the megaclasts contain folds and normal faults, indicating that they have undergone severe internal deformation during their downslope movement (Fig. 7a).

Remnant blocks show little internal deformation and vertical stratigraphic continuity with underlying strata (Alves and Cartwright, 2009; Gamboa et al., 2011). They are considered to be in-situ portions of strata that were not remobilized during slope failure, which might be related to their harder lithologies, e.g., limestones, and cemented siliciclastic sediment (Mohriak et al., 2008). Remnant blocks are laterally bounded by faults propagating from underlying strata and their bases do not show any significant disruption (e.g., Gamboa et al., 2011). However, most (76.7%) of the remnant megaclasts (Type II) identified in this study are observed to be tilted and/or internally deformed (Fig. 7b, Table 5). In addition, some of the remnant megaclasts show some degree of erosion at their bases, especially in their frontal parts (Figs. 7b, 10d). This suggests that these remnant megaclasts might have been moved for a quite limited distance, pushed by the surrounding mass wasting strata or by other moving megaclasts (Fig. 13d-e; Vanneste et al., 2006). Therefore, the significant differences between the remnant and transported megaclasts in terms of their scales, degree of internal deformation and external rotation can be attributed to their different emplacement processes. Finally, the strata below the megaclasts would have been deformed due to compaction after their emplacement, leading to the formation of Type II depressions (Fig. 13f).

We recognize some limitations in the approach we used to quantify the morphological parameters of megaclasts within MTCs. The vertical exaggeration (V.E.) and vertical scale of seismic profiles may influence the actual observed shapes and internal architectures of megaclasts. However, it is not possible to conduct a time/depth conversion to show the real vertical scale on the seismic profiles due to the lack of velocity values for the interval of interest, especially for the megaclasts. As for the vertical exaggeration, we use a constant valve of 5:1 for all the seismic profiles we used in this study. All these caveats should be taken in consideration by interpreters and structural geologists when analyzing megaclasts in seismic data.

6 Conclusions

We use high-resolution 3D seismic reflection data to investigate the morphological and seismic characteristics of 123 megaclasts within a mass-transport complex in the deep-water Taranaki Basin, offshore New Zealand. The main conclusions of this work are:

(1) Megaclasts are characterized by moderate-to-high amplitude seismic reflections and can reach up to 1900 m in length, ca. 1200 m in width and ca. 400 m in height.

(2) In seismic data, the internal reflections or strata in megaclasts appear rotated and deformed.

(3) A new morphometric classification of megaclasts is based on the deformational styles in terms of internal deformation and external rotation. Hence, megaclasts in the study area are quantitatively divided into four types: undeformed, rotated, deformed, and highly deformed.

(4) The two different kinds of depressions formed at the basal shear zones indicate if the megaclasts in MTC 2 are either transported or remnant.

(5) Downslope movement of large slide blocks or megaclasts during mass wasting can promote erosion of their underlying strata and internal deformation.

This work quantitatively clarifies the relationships between the deformational styles of megaclasts and the basal shear zone, which is better for understanding the emplacement processes of megaclasts along many continental margins. Our approach is able to reflect the relatively different types of megaclasts in terms of their internal deformation and angle of rotation.

Acknowledgments

We thank New Zealand Crown Research Institute (GNS Science) for providing the Romney 3D survey, well data and report for this work (https://data.nzpam.govt.nz/). This work was financially supported by the Key Special Project for Introduced Talents Team of Southern Marine Science and Engineering Guangdong Laboratory (Guangzhou) (GML2019ZD0104), Guangdong Basic and Applied Basic Research Foundation (2020B1515020016) and National Natural Science Foundation of China (41876054 and 41976077). Dr. Wei Li is funded by CAS Pioneer Hundred Talents Program (Y8SL011001). Two reviewers, Kei Ogata and Julien Bailleul, Associate Editor Stefano Mazzoli and Science Editor Mihai Ducea are acknowledged for their constructive comments, which greatly improved the manuscript.

Data Availability

The seismic and well data that support the findings of this study are available upon request from https://data.nzpam.govt.nz/GOLD/system/mainframe.asp.

References

Alves, T. M., 2010, 3D Seismic examples of differential compaction in mass-transport deposits and their effect on post-failure strata: Marine Geology, v. 271, no. 3-4, p. 212-224.

Alves, T. M., 2015, Submarine slide blocks and associated soft-sediment deformation in deep-water basins: A review: Marine and Petroleum Geology, v. 67, p. 262-285.

Alves, T. M., and Cartwright, J. A., 2009, Volume balance of a submarine landslide in the Espírito Santo Basin, offshore Brazil: quantifying seafloor erosion, sediment accumulation and depletion: Earth Planetary Science Letters, v. 288, no. 3-4, p. 572-580.

Beavan, J., Tregoning, P., Bevis, M., Kato, T., and Meertens, C., 2002, Motion and rigidity of the Pacific Plate and implications for plate boundary deformation: Journal of Geophysical Research: Solid Earth, v. 107, no. B10, p. ETG 19-11-ETG 19-15.

Bull, S., Arnot, M., Browne, G., Crundwell, M., Nicol, A., and Strachan, L., 2019, Neogene and Quaternary Mass-Transport Deposits From the Northern Taranaki Basin (North Island, New Zealand) Morphologies, Transportation Processes, and Depositional Controls: Submarine Landslides: Subaqueous Mass Transport Deposits from Outcrops to Seismic Profiles, p. 171-180.

Bull, S., Browne, G. H., Arnot, M. J., and Strachan, L. J., 2020, Influence of mass transport deposit (MTD) surface topography on deep-water deposition: an example from a predominantly fine-grained continental margin, New Zealand: Geological Society, London, Special Publications, v. 500, no. 1, p. 147-171.

Bull, S., Cartwright, J., and Huuse, M., 2009, A review of kinematic indicators from mass-transport complexes using 3D seismic data: Marine Petroleum Geology, v. 26, no. 7, p. 1132-1151.

Canals, M., Lastras, G., Urgeles, R., Casamor, J., Mienert, J., Cattaneo, A., De Batist, M., Haflidason, H., Imbo, Y., and Laberg, J., 2004, Slope failure dynamics and impacts from seafloor and shallow sub-seafloor geophysical data: case studies from the COSTA project: Marine Geology, v. 213, no. 1-4, p. 9-72.

Cardona, S., Wood, L. J., Dugan, B., Jobe, Z., Strachan, L. J., and Baas, J., 2020, Characterization of the Rapanui mass-transport deposit and the basal shear zone: Mount Messenger Formation, Taranaki Basin, New Zealand: Sedimentology, v. 67, no. 4, p. 2111-2148.

Collot, J.-Y., Lewis, K., Lamarche, G., and Lallemand, S., 2001, The giant Ruatoria debris avalanche on the northern Hikurangi margin, New Zealand: Result of oblique seamount subduction: Journal of Geophysical Research: Solid Earth, v. 106, no. B9, p. 19271-19297.

Cooper, R. A., Crampton, J. S., Raine, J. I., Gradstein, F. M., Morgans, H. E., Sadler, P. M., Strong, C. P., Waghorn, D., and Wilson, G. J., 2001, Quantitative biostratigraphy of the Taranaki Basin, New Zealand: a deterministic and probabilistic approach: AAPG bulletin, v. 85, no. 8, p. 1469-1498.

Cox, D. R., Huuse, M., Newton, A. M. W., Gannon, P., and Clayburn, J., 2020, Slip sliding away: Enigma of large sandy blocks within a gas-bearing mass transport deposit, offshore northwestern Greenland: AAPG Bulletin, v. 104, no. 5, p. 1011-1043.

Deptuck, M., Mosher, D., Campbell, D., Hughes-Clarke, J., and Noseworthy, D., 2007, Along slope variations in mass failures and relationships to major Plio-Pleistocene morphological elements, SW Labrador Sea, Submarine mass movements and their consequences, Springer, p. 37-45.

Draganits, E., Schlaf, J., Grasemann, B., and Argles, T., 2008, Giant submarine landslide grooves in the Neoproterozoic/Lower Cambrian Phe Formation, northwest Himalaya: Mechanisms of formation and palaeogeographic implications: Sedimentary Geology, v. 205, no. 3-4, p. 126-141.

Gamboa, D., Alves, T., and Cartwright, J., 2011, Distribution and characterization of failed (mega) blocks along salt ridges, southeast Brazil: Implications for vertical fluid flow on continental margins: Journal of Geophysical Research: Solid Earth, v. 116, no. B8, p. 1-20.

Gamboa, D., Alves, T., and Cartwright, J., 2012, Seismic-scale rafted and remnant blocks over salt ridges in the Espírito Santo Basin, Brazil, Submarine mass movements and their consequences, Springer, p. 629-638.

Gamboa, D., and Alves, T. M., 2015, Three-dimensional fault meshes and multi-layer shear in mass-transport blocks: Implications for fluid flow on continental margins: Tectonophysics, v. 647-648, p. 21-32.

Gee, M. J. R., Gawthorpe, R., and Friedmann, J., 2005, Giant striations at the base of a submarine landslide: Marine Geology, v. 214, no. 1-3, p. 287-294.

Giba, M., Nicol, A., and Walsh, J. J., 2010, Evolution of faulting and volcanism in a back-arc basin and its implications for subduction processes: Tectonics, v. 29, no. 4, p. 1-18.

Hampton, M. A., Lee, H. J., and Locat, J., 1996, Submarine landslides: Reviews of Geophysics, v. 34, no. 1, p. 33-59.

Hansen, R. J., and Kamp, P. J., 2002, Evolution of the Giant Foresets Formation, northern Taranaki Basin, New Zealand, p. 419-499.

Hansen, R. J., and Kamp, P. J. J., 2006, An integrated biostratigraphy and seismic stratigraphy for the late Neogene continental margin succession in northern Taranaki Basin, New Zealand: New Zealand Journal of Geology and Geophysics, v. 49, no. 1, p. 39-56.

Higgs, K., King, P., Raine, J., Sykes, R., Browne, G., Crouch, E., and Baur, J., 2012, Sequence stratigraphy and controls on reservoir sandstone distribution in an Eocene marginal marine-coastal plain fairway, Taranaki Basin, New Zealand: Marine Petroleum Geology, v. 32, no. 1, p. 110-137.

Hodgson, D. M., Brooks, H. L., Ortiz-Karpf, A., Spychala, Y., Lee, D. R., and Jackson, C. A. L., 2019, Entrainment and abrasion of megaclasts during submarine landsliding and their impact on flow behaviour: Geological Society, London, Special Publications, v. 477, no. 1, p. 223-240.

Holt, W. E., and Stern, T. A., 1994, Subduction, platform subsidence, and foreland thrust loading: The late Tertiary development of Taranaki Basin, New Zealand: Tectonics, v. 13, p. 1068-1092.

Hunt, J. E., Tappin, D. R., Watt, S. F. L., Susilohadi, S., Novellino, A., Ebmeier, S. K., Cassidy, M., Engwell, S. L., Grilli, S. T., Hanif, M., Priyanto, W. S., Clare, M. A., Abdurrachman, M., and Udrekh, U., 2021, Submarine landslide megablocks show half of Anak Krakatau island failed on December 22nd, 2018: Nature Communications, v. 12, no. 1, p. 1-15.

Huvenne, V. A., Croker, P. F., and Henriet, J. P., 2002, A refreshing 3D view of an ancient sediment collapse and slope failure: Terra Nova, v. 14, no. 1, p. 33-40.

Infante-Paez, L., and Marfurt, K. J., 2017, Seismic expression and geomorphology of igneous bodies: A Taranaki Basin, New Zealand, case study: Interpretation, v. 5, no. 3, p. SK121-SK140.

Jackson, C. A. L., 2011, Three-dimensional seismic analysis of megaclast deformation within a mass transport deposit; implications for debris flow kinematics: Geology, v. 39, no. 3, p. 203-206.

Joanne, C., Lamarche, G., and Collot, J. Y., 2013, Dynamics of giant mass transport in deep submarine environments: the Matakaoa Debris Flow, New Zealand: Basin Research, v. 25, no. 4, p. 471-488.

Johnson, D. L., 1970, A general model for the intermediate stage of sintering: Journal of the American Ceramic Society, v. 53, no. 10, p. 574-577.

Kamp, P. J. J., Vonk, A. J., Bland, K. J., Hansen, R. J., Hendy, A. J. W., McIntyre, A. P., Ngatai, M., Cartwright, S. J., Hayton, S., and Nelson, C. S., 2004, Neogene stratigraphic architecture and tectonic evolution of Wanganui, King Country, and eastern Taranaki Basins, New Zealand: New Zealand Journal of Geology and Geophysics, v. 47, no. 4, p. 625-644.

King, P. R., and Thrasher, G. P., 1992, Post-Eocene development of the Taranaki Basin, New Zealand: Convergent overprint of a passive margin: Chapter 7: Southwest Pacific and Eastern Indian Ocean Margins, p. 93-118.

Kumar, P. C., Omosanya, K. d. O., Eruteya, O. E., and Sain, K., 2021, Geomorphological characterization of basal flow markers during recurrent mass movement: A case study from the Taranaki Basin, offshore New Zealand: Basin Research, v. 33, no. 4, p. 2358-2382.

Lastras, G., De Blasio, F. V., Canals, M., and Elverhøi, A., 2005, Conceptual and numerical modeling of the BIG'95 debris flow, western Mediterranean Sea: Journal of Sedimentary Research, v. 75, no. 5, p. 784-797.

Lee, H., Ryan, H., Kayen, R. E., Haeussler, P. J., Dartnell, P., and Hampton, M. A., 2006, Varieties of submarine failure morphologies of seismically-induced landslides in Alaskan fjords: Norwegian Journal of Geology/Norsk Geologisk Forening, v. 86, no. 3, p. 221-230.

Lucente, C. C., and Pini, G. A., 2003, Anatomy and emplacement mechanism of a large submarine slide within a Miocene foredeep in the northern Apennines, Italy: A field perspective: American Journal of Science, v. 303, no. 7, p. 565-602.

Masson, D., Huggett, Q., and Brunsden, D., 1993, The surface texture of the Saharan debris flow deposit and some speculations on submarine debris flow processes: Sedimentology, v. 40, no. 3, p. 583-598.

Mitchum Jr, R., Vail, P. R., and Thompson III, S., 1977, Seismic stratigraphy and global changes of sea level: Part 2. The depositional sequence as a basic unit for stratigraphic analysis: Section 2. Application of seismic reflection configuration to stratigraphic interpretation, p. 53-62.

Mohriak, W., Nemčok, M., and Enciso, G., 2008, South Atlantic divergent margin evolution: rift-border uplift and salt tectonics in the basins of SE Brazil: Geological Society, London, Special Publications, v. 294, no. 1, p. 365-398.

Moore, J. G., Bryan, W. B., Beeson, M. H., and Normark, W. R., 1995, Giant blocks in the South Kona landslide, Hawaii: Geology, v. 25, p. 125–128.

Moscardelli, L., and Wood, L., 2008, New classification system for mass transport complexes in offshore Trinidad: Basin research, v. 20, no. 1, p. 73-98.

Nisbet, E. G., and Piper, D. J., 1998, Giant submarine landslides: Nature, v. 392, no. 6674, p. 329-330.

Nwoko, J., Kane, I., and Huuse, M., 2020a, Mass transport deposit (MTD) relief as a control on post-MTD sedimentation: Insights from the Taranaki Basin, offshore New Zealand: Marine and Petroleum Geology, v. 120, p. 1-12.

Nwoko, J., Kane, I., and Huuse, M., 2020b, Megaclasts within mass-transport deposits: their origin, characteristics and effect on substrates and succeeding flows: Geological Society, London, Special Publications, v. 500, no. 1, p. 515-530.

Ogata, K., Festa, A., and Pini, G. A., 2020, Submarine Landslides: subaqueous mass transport deposits from outcrop to seismic profiles, p. 1-384.

Ogata, K., Festa, A., Pini, G. A., and Alonso, J. L., 2019, Submarine landslide deposits in orogenic belts: olistostromes and sedimentary mélanges: Submarine Landslides: Subaqueous Mass Transport Deposits from Outcrops to Seismic Profiles, p. 1-26.

Ogata, K., Pini, G. A., Festa, A., Pogačnik, Ž., Tunis, G., Mountjoy, J. J., Senger, K., and Strasser, M., 2014, High-Resolution Studies of Mass Transport Deposits: Outcrop Perspective for Understanding Modern Submarine Slope Failure and Associated Natural Hazards, Engineering Geology for Society and Territory – Volume 4, p. 209-213.

Omeru, T., 2014, Mass transport deposits: implications for reservoir seals [Doctoral thesis]: Cardiff University, p. 97-277.

Omeru, T., and Cartwright, J. A., 2019, The efficacy of kinematic indicators in a complexly deformed Mass Transport Deposit: Insights from the deepwater Taranaki Basin, New Zealand: Marine and Petroleum Geology, v. 106, p. 74-87.

Omosanya, K. O., 2018, Episodic fluid flow as a trigger for Miocene-Pliocene slope instability on the Utgard High, Norwegian Sea: Basin Research, v. 30, no. 5, p. 942-964.

Omosanya, K. O., and Alves, T. M., 2013, A 3-dimensional seismic method to assess the provenance of Mass-Transport Deposits (MTDs) on salt-rich continental slopes (Espírito Santo Basin, SE Brazil): Marine and Petroleum Geology, v. 44, p. 223-239.

Ortiz-Karpf, A., Hodgson, D. M., Jackson, C. A. L., and McCaffrey, W. D., 2017, Influence of Seabed Morphology and Substrate Composition On Mass-Transport Flow Processes and Pathways: Insights From the Magdalena Fan, Offshore Colombia: Journal of Sedimentary Research, v. 87, no. 3, p. 189-209.

Ortiz-Karpf, A., Hodgson, D. M., and McCaffrey, W. D., 2015, The role of mass-transport complexes in controlling channel avulsion and the subsequent sediment dispersal patterns on an active margin: The Magdalena Fan, offshore Colombia: Marine and Petroleum Geology, v. 64, p. 58-75.

Rad, F. J. M. o. E. D. N. Z. U. P. R., PR, 2015, Romney-1 Well Completion Report, v. 980.

Rusconi, F. J., 2017, 3D seismic interpretation of a Plio-Pleistocene mass transport deposit in the deepwater Taranaki Basin of New Zealand, Arkansas [Master thesis]: University of Arkansas, 2583.Scarselli, N., 2020, Submarine landslides – architecture, controlling factors and environments. A summary, Regional Geology and Tectonics: Principles of Geologic Analysis, p. 417-439.

Scott, G., King, P., and Crundwell, M., 2004, Recognition and interpretation of depositional units in a late Neogene progradational shelf margin complex, Taranaki Basin, New Zealand: foraminiferal data compared with seismic facies and wireline logs: Sedimentary Geology, v. 164, no. 1-2, p. 55-74.

Soutter, E. L., Kane, I. A., and Huuse, M., 2018, Giant submarine landslide triggered by Paleocene mantle plume activity in the North Atlantic: Geology, v. 46, no. 6, p. 511-514.

Stagpoole, V., and Nicol, A., 2008, Regional structure and kinematic history of a large subduction back thrust: Taranaki Fault, New Zealand: Journal of Geophysical Research, v. 113, no. B1, p. 1-5.

Strogen, D. P., Higgs, K. E., Griffin, A. G., and Morgans, H. E. G., 2019, Late Eocene – Early Miocene facies and stratigraphic development, Taranaki Basin, New Zealand: the transition to plate boundary tectonics during regional transgression: Geological Magazine, v. 156, no. 10, p. 1751-1770.

Strogen, D. P., Seebeck, H., Nicol, A., and King, P. R., 2017, Two-phase Cretaceous–Paleocene rifting in the Taranaki Basin region, New Zealand; implications for Gondwana break-up: Journal of the Geological Society, v. 174, no. 5, p. 929-946.

Tinti, S., Bortolucci, E., and Vannini, C., 1997, A Block-Based Theoretical Model Suited to Gravitational Sliding: Natural Hazards, v. 16, p. 1–28.

Vanneste, M., Mienert, J., and Bünz, S., 2006, The Hinlopen Slide: A giant, submarine slope failure on the northern Svalbard margin, Arctic Ocean Earth and Planetary Science Letters, v. 245, no. 1, p. 373–388.

Ward, N. I. P., Alves, T. M., and Blenkinsop, T. G., 2018, Submarine sediment routing over a blocky mass-transport deposit in the Espírito Santo Basin, SE Brazil: Basin Research, v. 30, no. 4, p. 816-834.

Wu, N., Jackson, C. A.-L., Johnson, H., Hodgson, D. M., Clare, M., Nugraha, H. D., and Li, W., 2021, The formation and implications of giant blocks and fluid escape structures in submarine lateral spreads: Basin Research, v. 33, no. 3, p. 1711-1730.

Figures

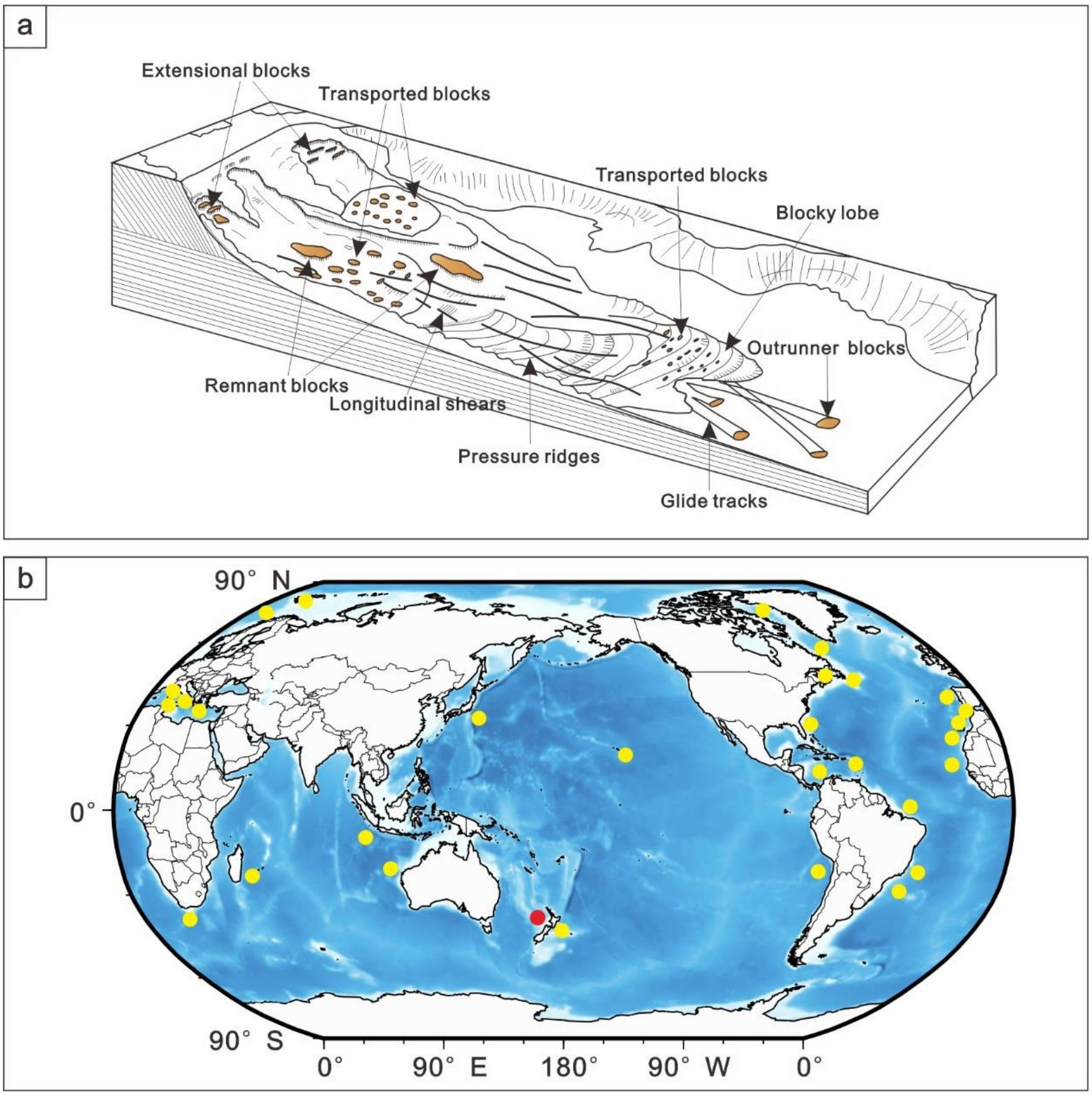

Fig. 1 (a) Model for mass-transport complexes (MTCs) showing four types of blocks: extensional blocks, remnant blocks, transport blocks and outrunner blocks (figure adapted from Nissen et al., 1999). (b) Global distribution of blocky MTCs (yellow dots, modified from Alves, 2015) and the location of the study area (red circle).

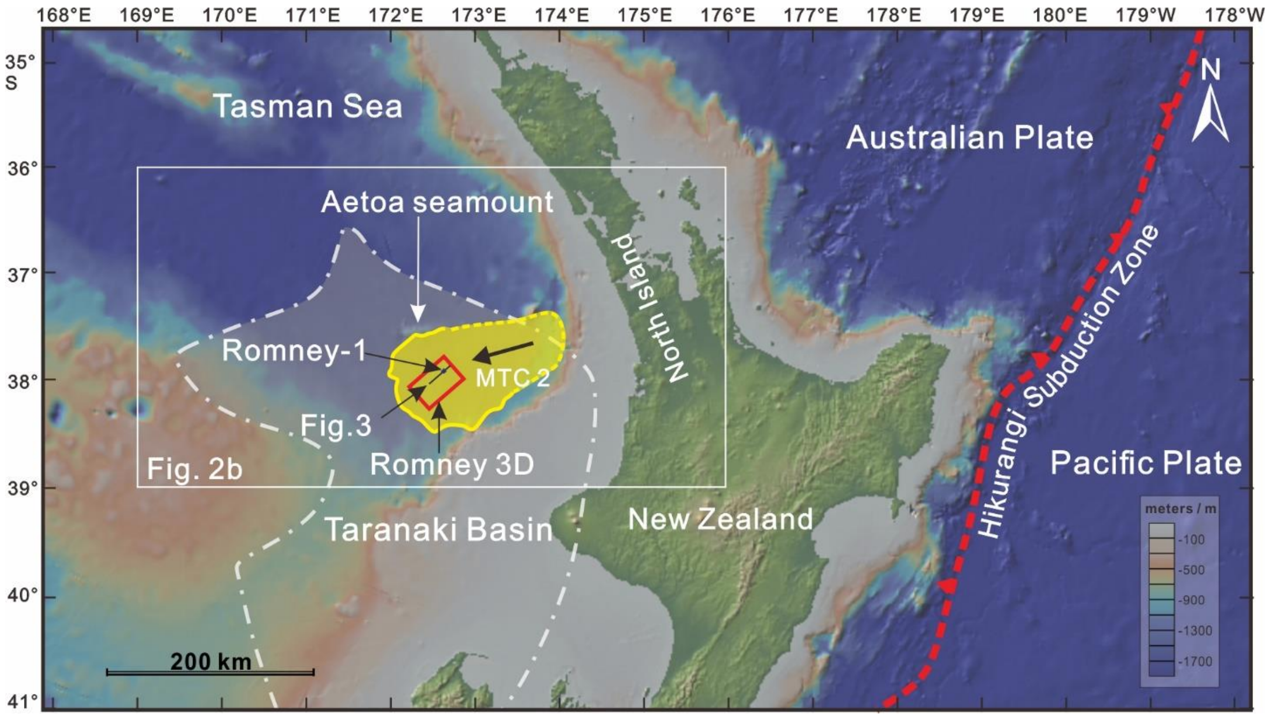

Fig. 2 Topographic map showing main structural elements (Australian Plate, Pacific Plate and Hikurangi Subduction Zone), location of the Taranaki Basin (figure adapted from Strogen et al., 2017), the distribution of MTC 2 (marked in yellow; figure modified from Omeru et al., 2014), and the study area (red box), located in the translational domain of MTC 2.

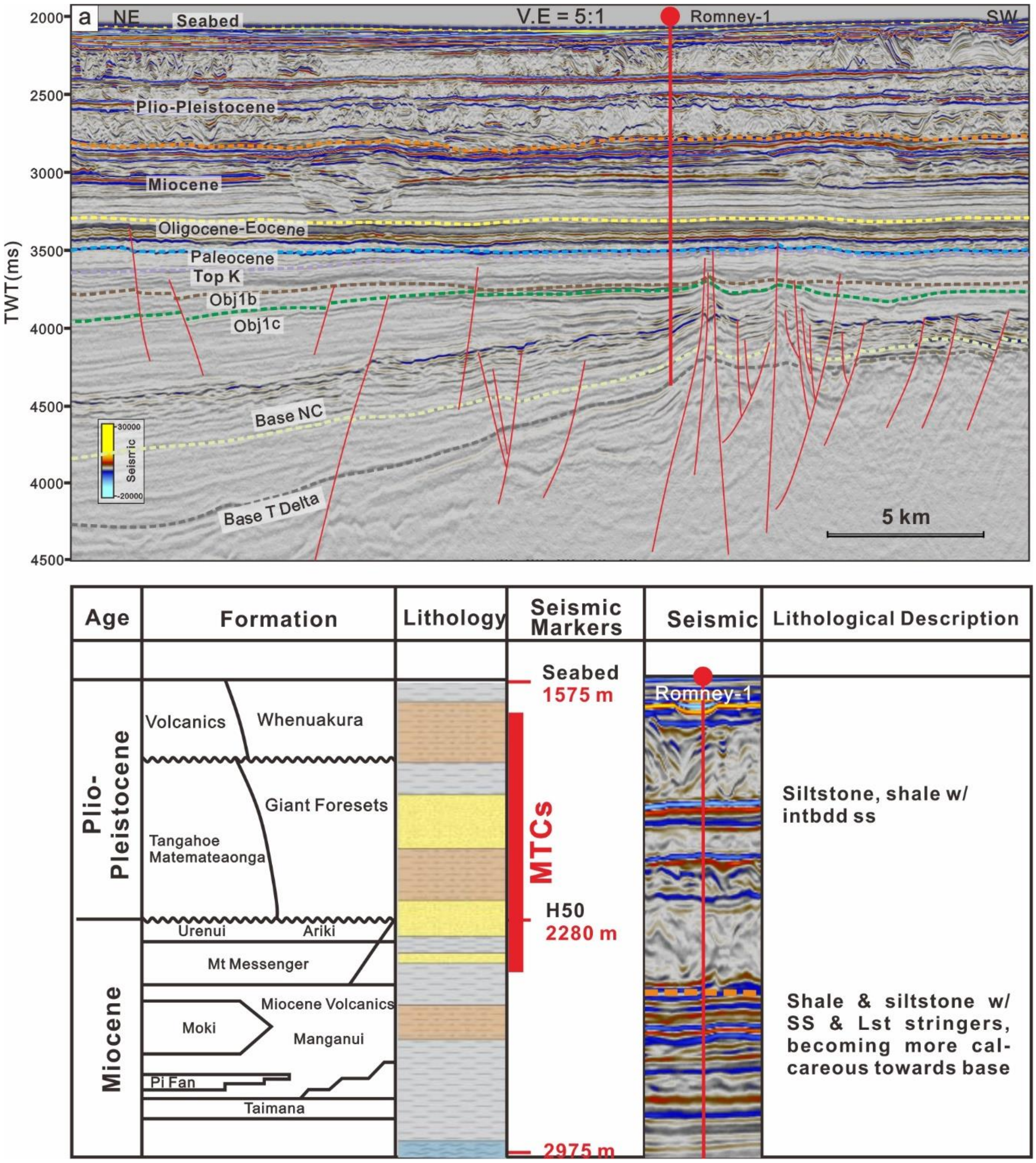

Fig. 3 (a) Interpreted seismic profile crossing well Romney-1 showing regional seismic-stratigraphy units and the eight (8) seismic horizons that bound them (figure modified from Bull et al., 2020). The location of seismic profile is shown in Fig. 2b. (b) Lithological column highlighting the stratigraphic succession intersected by well Romney-1.

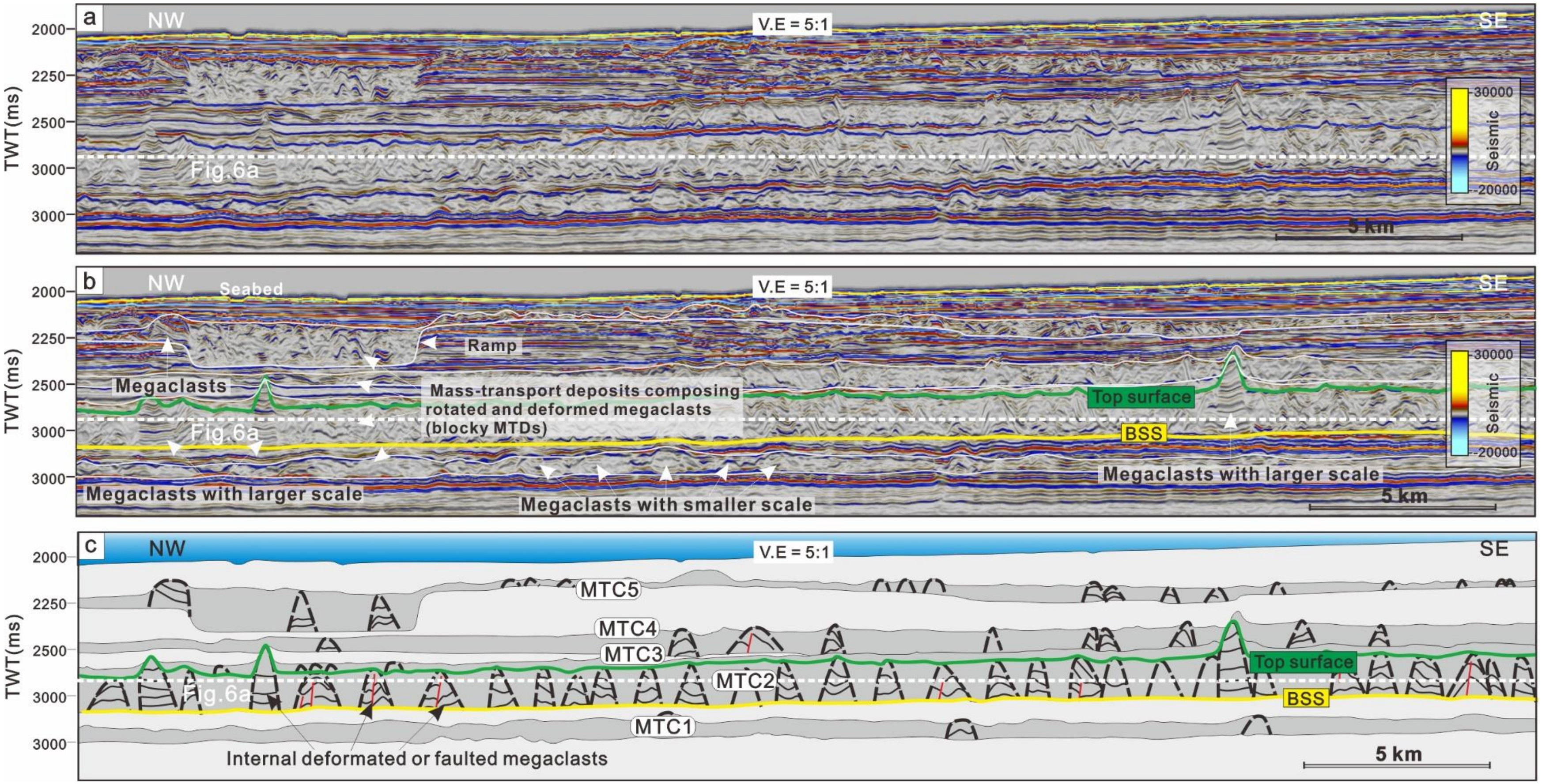

Fig. 4 (a) Uninterpreted regional seismic profile. (b) Interpretation of the regional seismic profiles showing megaclasts of different sizes within MTCs. VE: Vertical Exaggeration. BSS: basal shear surface. (c) interpretation on the seismic profiles shown above.

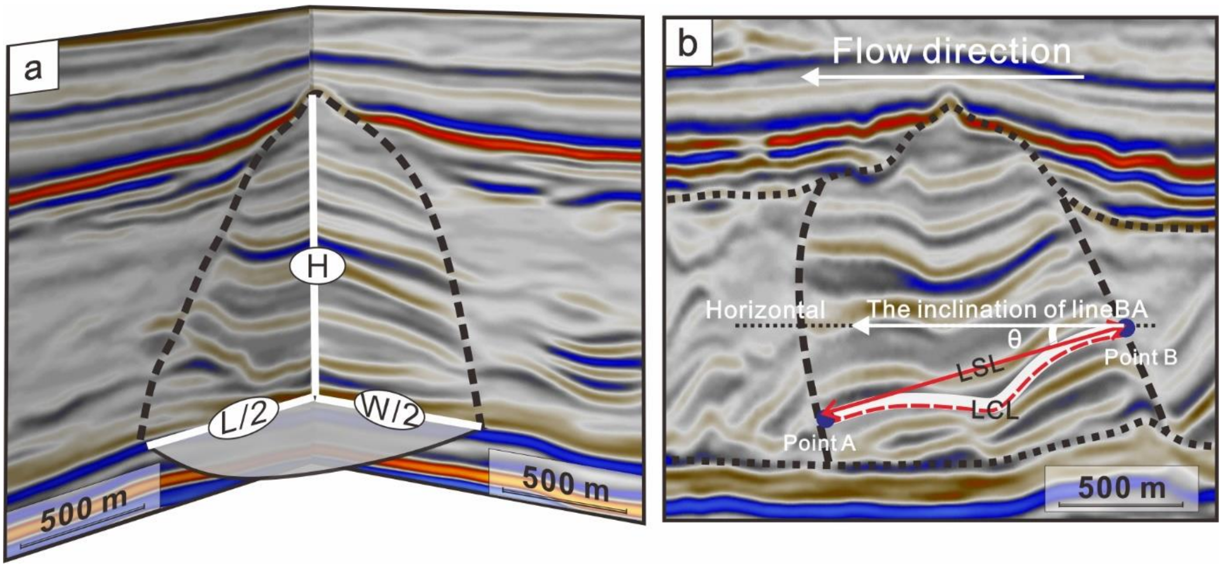

Fig. 5 (a) Geometric parameters measured for the megaclasts include length (L), width (W) and height (H). (b) The 2D model of the megaclasts highlights their internal deformation. Note that the "LCL" represents the length of the curve line, corresponding to the true trace of reflection axis within megaclasts, the "LSL" represents the length of the straight line between the two points of the reflection axis, and "θ" represents the angle between the horizontal and the straight line between the two points of the reflection axis.

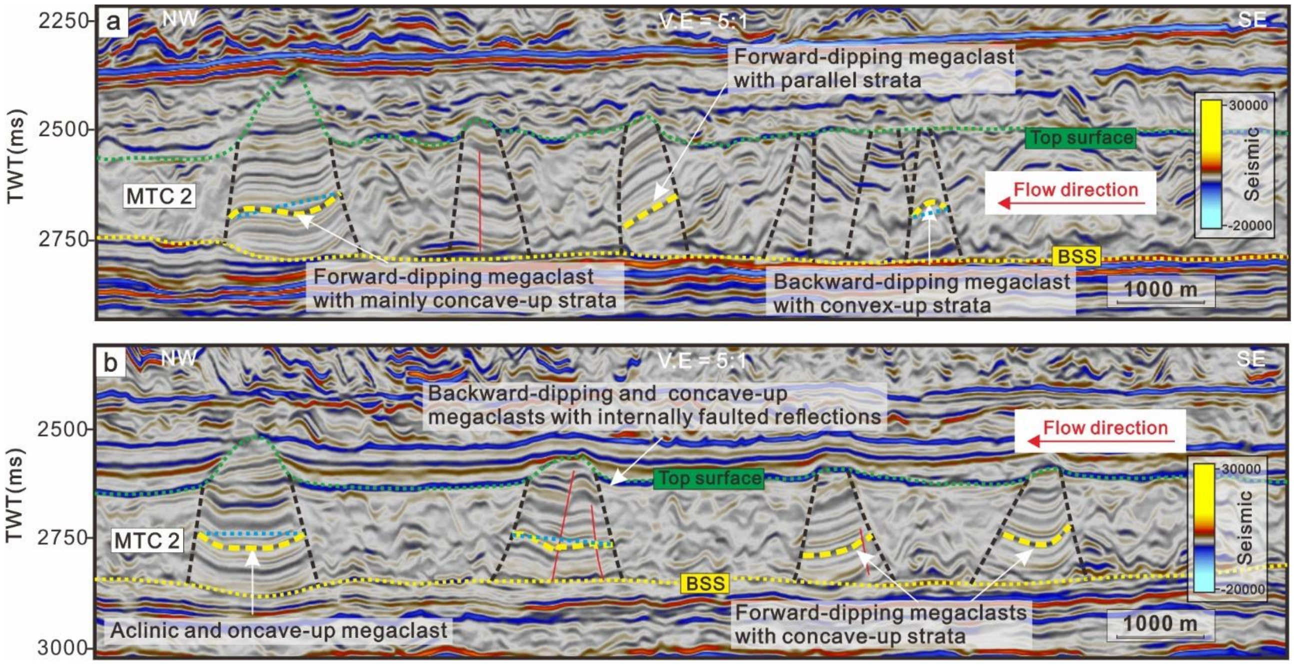

Fig. 6 Seismic profiles showing seismic characteristics of megaclasts within MTC 2 in the (a) eastern part and (b) western part of the study area. BSS: basal shear surface. Note that the yellow thick dotted lines within megaclasts indicate their deformation, while the blue thin dotted lines connect the two ends of the thick yellow dotted line and are used as a reference line to judge the external rotation and internal deformation of the megaclasts. BSS is basal shear surface.

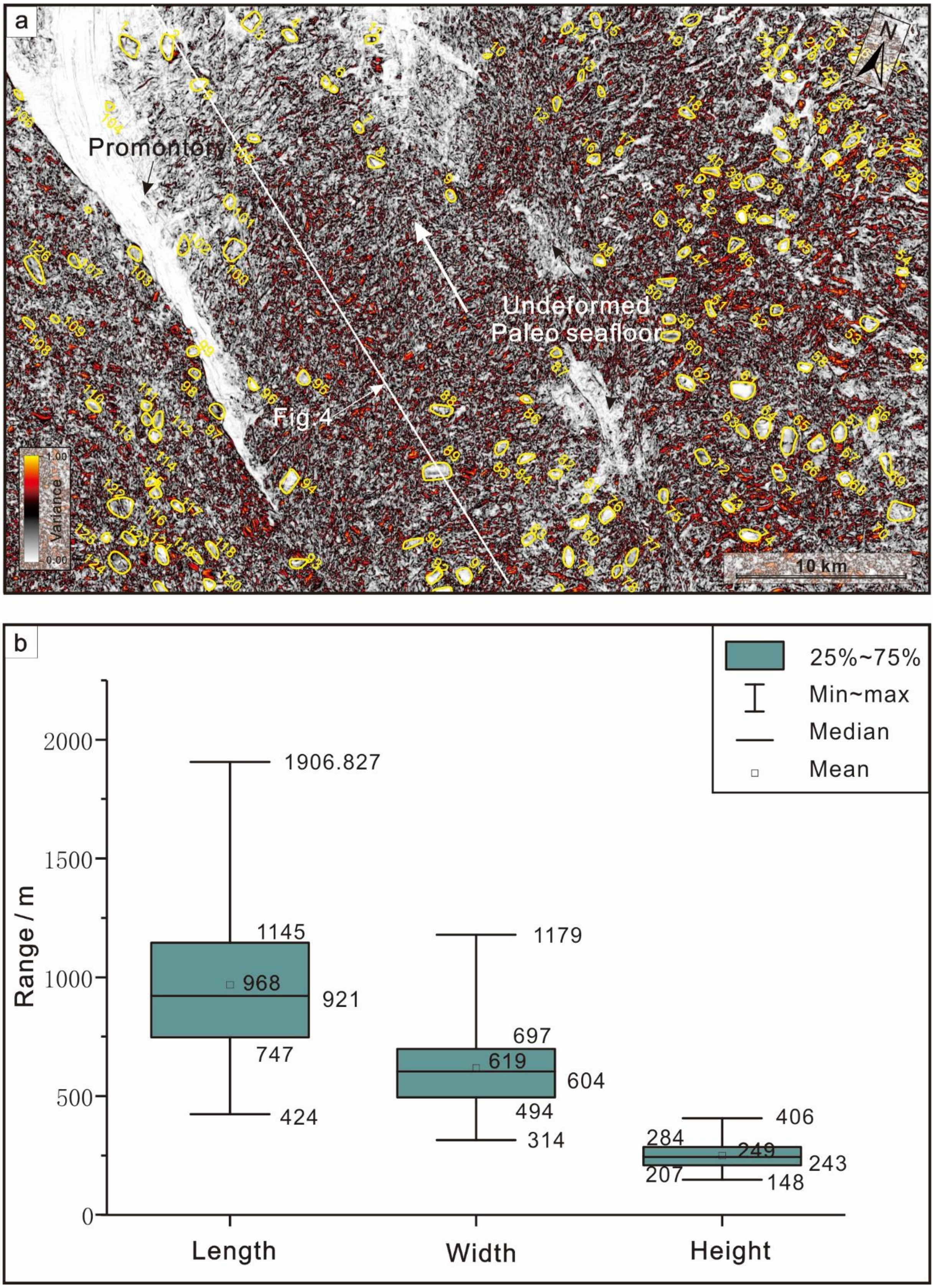

Fig. 7 (a) Time slice at T=2672 ms showing the distribution of megaclasts in MTC 2. The white arrow represents the sliding direction of MTC 2. The yellow lines indicate the boundaries of identified megaclasts in the study area. (b) Basic parameters of megaclasts in MTD 2 highlighting their length (L), width (W), and height (H).

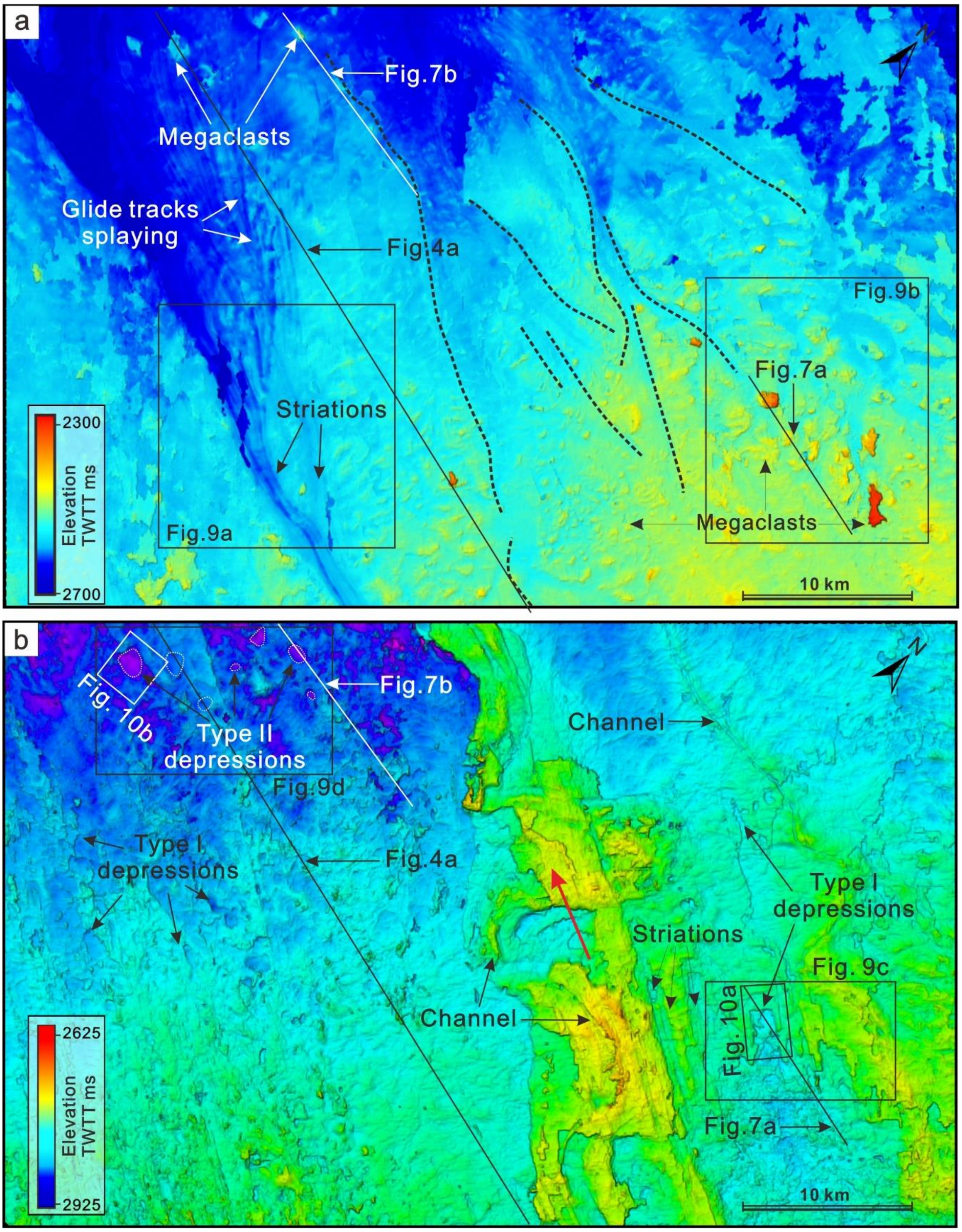

Fig. 8 (a) Structural map of the top MTC 2, showing the spatial distribution of megaclasts in the study area. At the NE part of the MTC 2, the rugged topographies at the top of the megaclasts created fairways associated with the deposition of the overlying MTC (i.e. MTC 3). While the NW part of the MTC 2 is characterized by glide tracks and striations associated with the translation of overlying MTC (i.e., MTC 3). (b) Structural map of the basal shear zone of MTC 2, showing the depressions and other geomorphological structures. Negative relief at the base of the MTC 2 is caused by channels. The red arrow represents the slip direction of MTC 2.

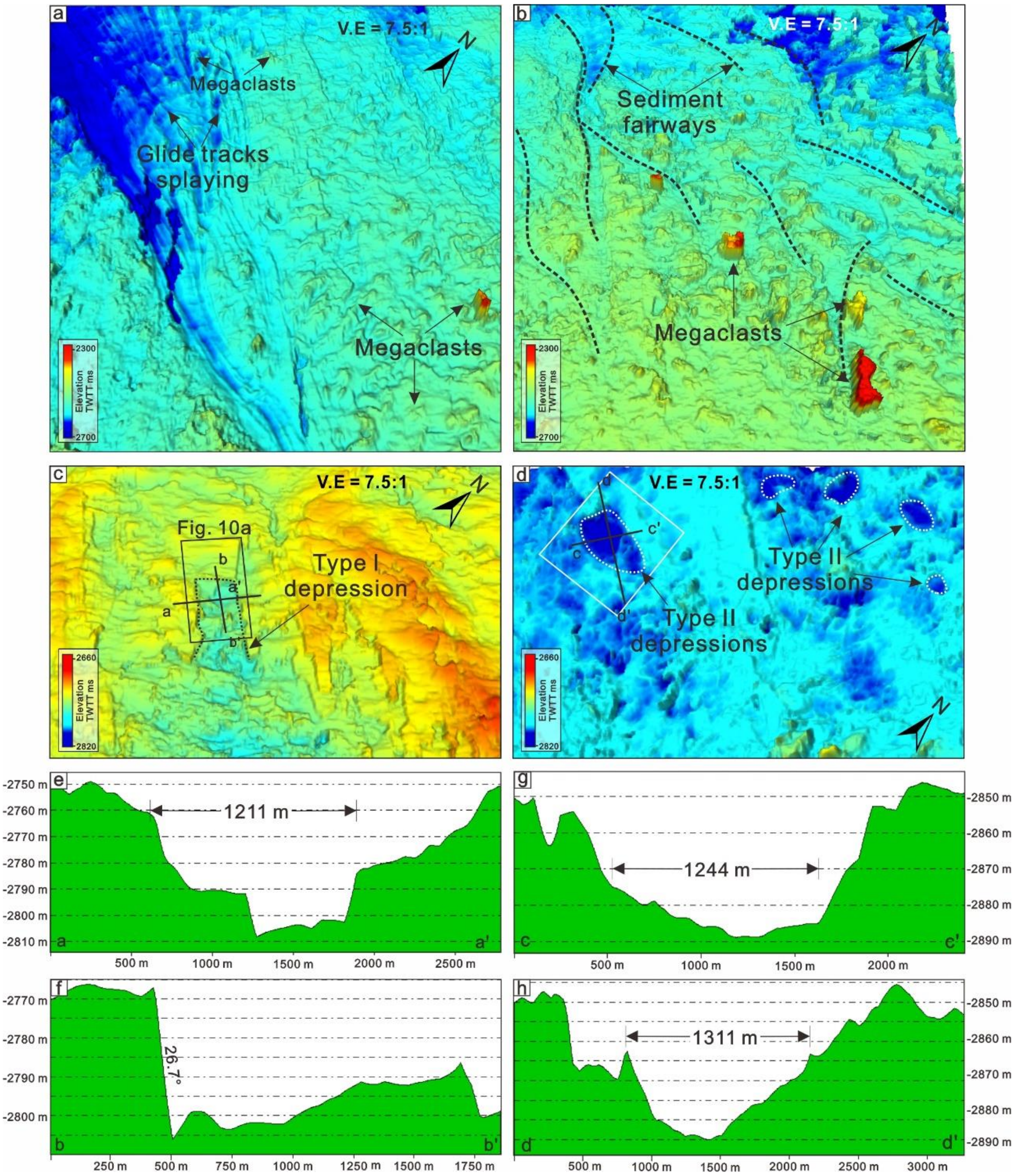

Fig. 9 3D view (a) Megaclasts and glide tracks at the top MTC 2 level and (b) sediment fairways created by the rugged topographies associated with the tops of the megaclasts. V.E refers to the high ratio of figure height and real high. Examples of (c) Type I and (d) Type II depressions associated with the base of the megaclasts. (e) and (f) Bathymetric profile of the type1 depressions shown in (c). (g) and (h) Bathymetric profile of the type 2 depressions shown in (d).

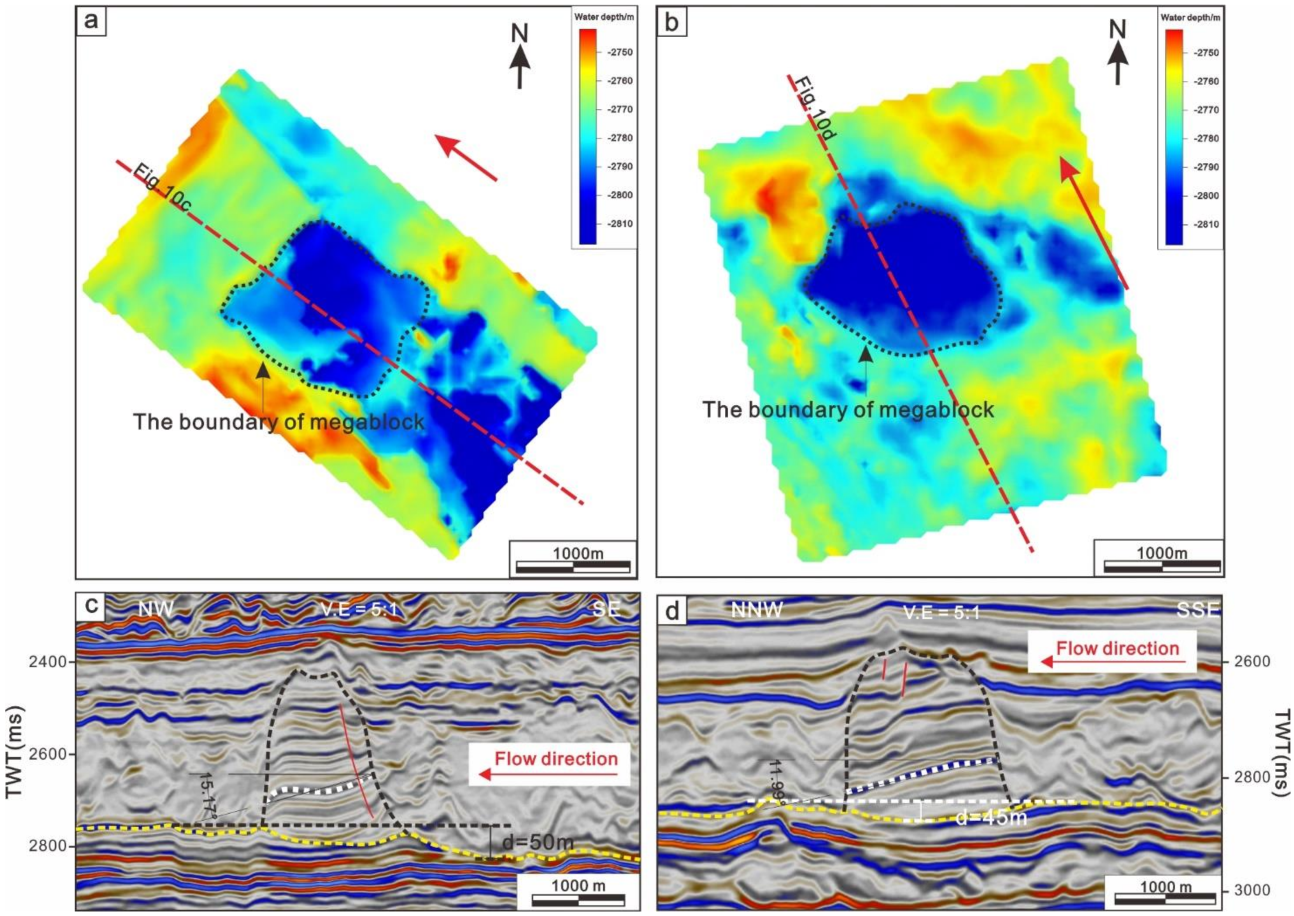

Fig. 10 (a) and (b) Time structural maps illustrate two different types of depressions on the basal shear zone of MTC 2. The boundaries of megaclasts are marked by black dotted circles. (c) and (d) Two-dimensional seismic profiles from three-dimensional seismic volume illustrating geometry and key internal deformation of megaclasts of figures 10a and b, respectively.

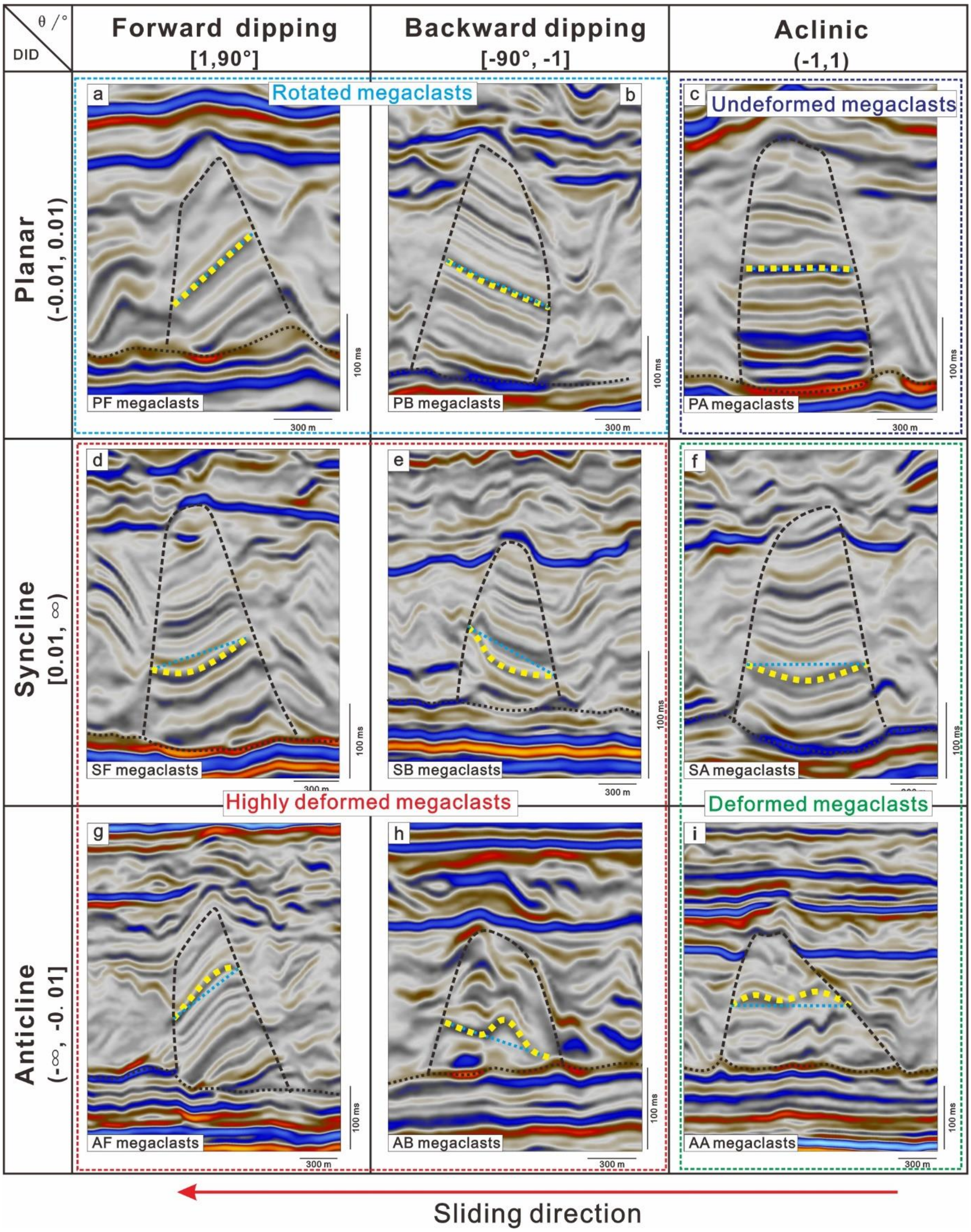

Fig. 11 New classification of megaclasts based on their angle of rotation (θ) and degree of deformation (DID) along the sliding direction. Note that the megaclasts can be quantitatively

classified into four main types: undeformed megaclasts, rotated megaclasts, deformed megaclasts and highly deformed megaclasts.

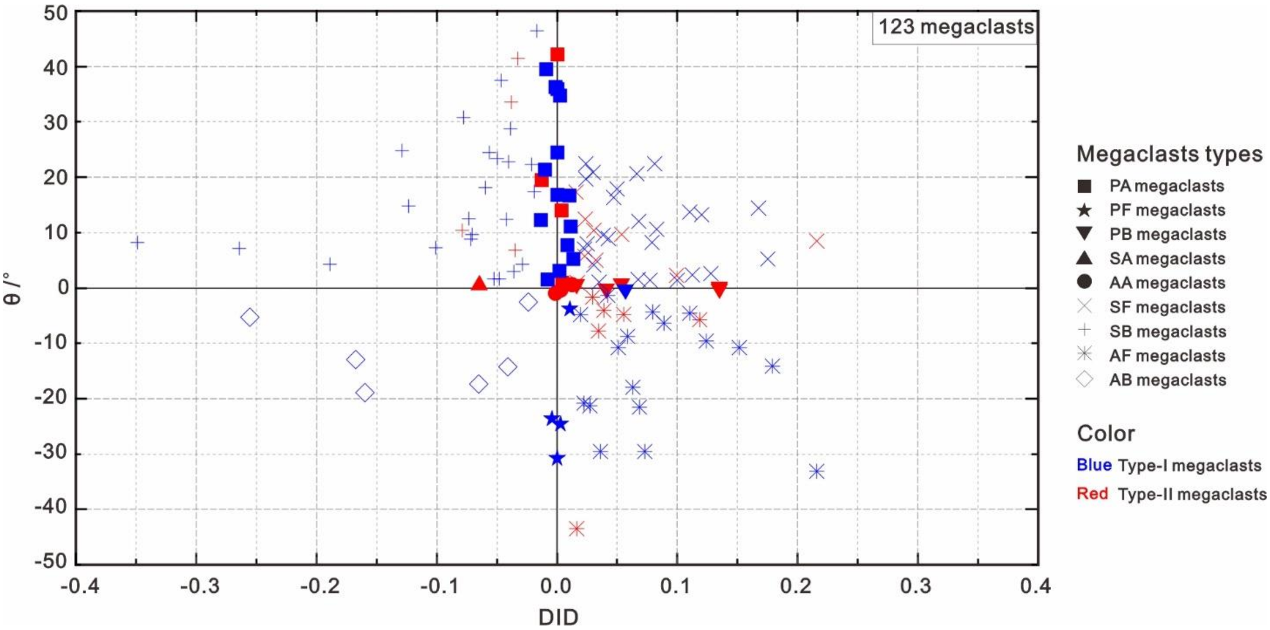

Fig. 12 Quantitative analysis of the deformational styles of megaclasts showing the internal deformation (DID) and rotation (θ) of 9 types of megaclasts with different symbols. Note that the blue symbols indicate the transported megaclasts and the red symbols represent the remnant megaclasts.

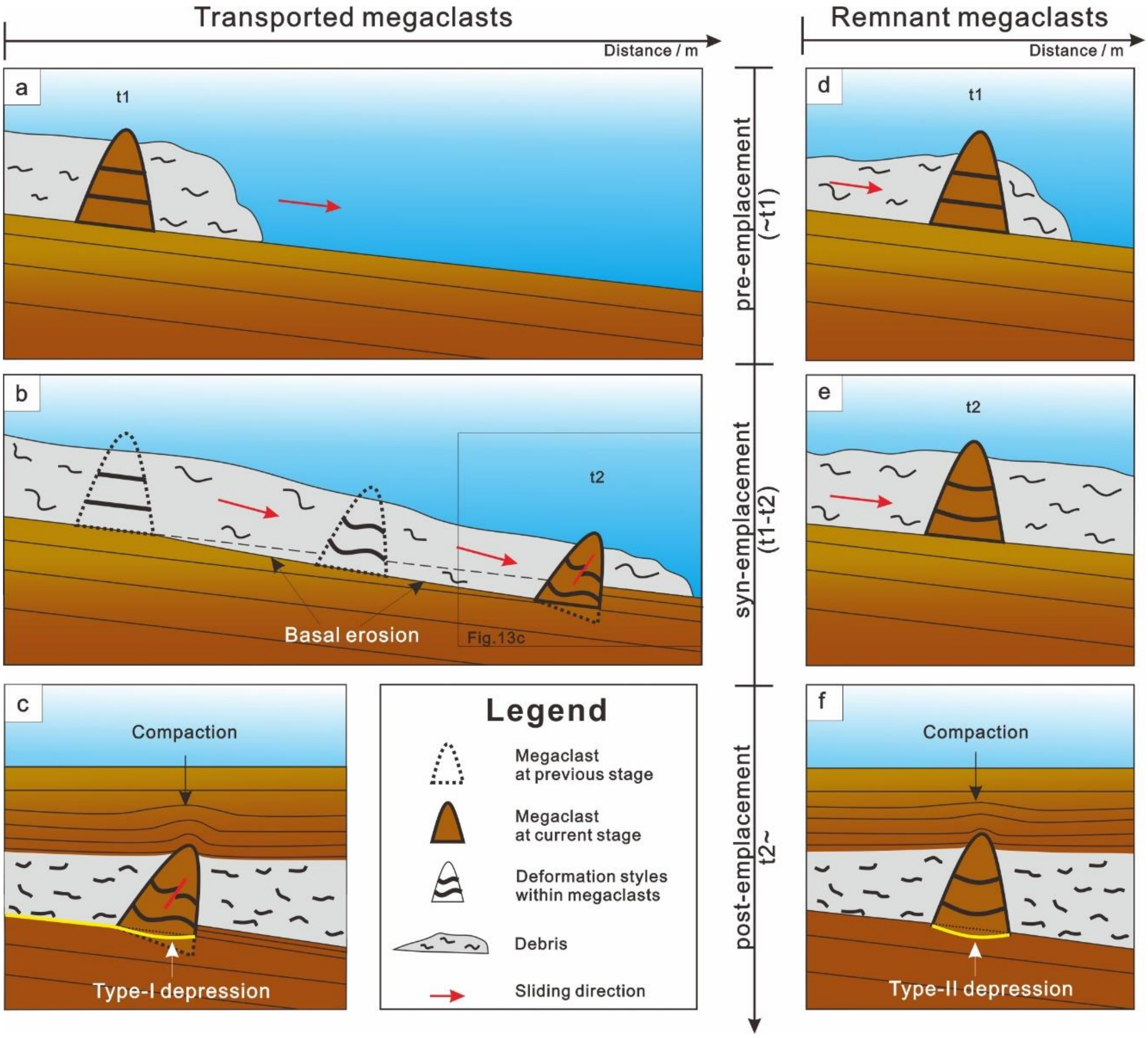

Fig. 13 Conceptual model shows the two different types of emplacement processes of megaclasts. (a) to (c) The transported megaclasts have eroded the underlying strata and produced the Type I (U-shaped) depressions during their emplacement. (d) to (f) Remnant megaclasts do not show obvious erosion at their bases and only leave Type II (circular-, oval- or irregular-shaped) depressions on the basal shear zone. Note that the emplacement processes of megaclasts can be divided into three stages (pre-, syn- and post-emplacement). Pre-emplacement (~t1): the internal structures within megaclasts are deformed (a) with the increasing sliding distance or (d) pushed by the surrounding mass-wasted chaotic strata and/or transported megaclasts. Syn-emplacement (t1-t2): (b) the transported megaclasts erode the basal shear zone and cease sliding; (e) the remnant megaclasts do not move or transport for

a quite limited distance. Post-emplacement (t2~): (c) and (f) Both types of the megaclasts are buried after their emplacement and circular depressions are generated on the basal shear zone due to compaction.